Surface Science 749 (2024) 122573

Contents lists available at ScienceDirect

Surface Science

journal homepage: www.elsevier.com/locate/susc

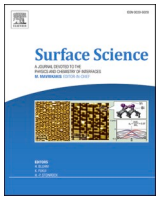

Reactivity of graphene-supported Co clusters

Natalie J. Waleska-Wellnhofer [a,1], Sophie Arzig [b,1], Fabian Düll [a], Udo Bauer [a], Phiona Bachmann [a], Johann Steinhauer [a], Christian Papp [a,b,*], Thomas Risse [b]

[a] Friedrich-Alexander-Universität, Erlangen-Nürnberg, Lehrstuhl für Physikalische Chemie II, Egerlandstr. 3, 91058 Erlangen, Germany
[b] Freie Universität Berlin, Physikalische und Theoretische Chemie, Arnimallee 22, 14195 Berlin, Germany

ARTICLE INFO

Keywords:
Supported nanocluster
Cluster chemistry
CO adsorption
Graphene
Cobalt

ABSTRACT

Graphene-supported Co clusters were investigated by high-resolution XPS, TPD and IRRAS using CO as a probe molecule. CO adsorption was observed at edge, on-top and bridge/hollow sites on the as-prepared clusters. Temperature-programmed XPS showed CO dissociation at $T > 300$ K. The CO desorption temperatures were determined by TPD measurements to be 260, 320 and 400 K for $CO^{bridge/hollow}$, CO^{edge} and CO^{top}, respectively. The CO dissociation products were used to investigate the adsorption of CO on carbon and oxygen precovered Co clusters. Site blocking by these adatoms was found resulting in the absence of CO^{edge} (XPS and TPD) and a decrease of the CO adsorption capacity (XPS, TPD and IRRAS). Additionally, no CO dissociation was found on the precovered clusters concluding a blocking of the catalytically active sites which are the edge sites of the clusters.

1. Introduction

In the industrial production of long chain hydrocarbons by the Fischer-Tropsch (FT) synthesis, cobalt and iron play an important role as catalytic active materials [1]. To improve the performance of these catalysts, it is crucial to understand the properties of the catalyst which make them suitable for the specific reaction. However, industrially used catalysts consist of many different components which make it hard to understand the reactivity of these systems. For instance, the cobalt containing catalysts in the FT reaction consist of 10 – 30 wt% cobalt, as well as a small amount of a second metal (noble metal) and an oxidic promoter supported on a metal oxide [1]. Since cobalt is found to be the catalytic active component of the catalyst, CO adsorption and dissociation on cobalt single crystal surfaces are excessively studied using various techniques, e.g., TPD, LEED, XPS, RAIRS [2–7]. Single crystal surfaces are the simplest model catalysts available. However, to gain information of the properties of such highly complex catalysts, model catalysts with increasing complexity have to be studied to overcome the material gap [8]. In this work, we investigated graphene-supported Co clusters. Here, graphene is used as a template, and as a model system for a carbon support. Due to the lattice mismatch of graphene on Rh(111), the graphene layer is corrugated [9]. This allows for the preparation of ordered nanocluster arrays with a narrow size distribution by depositing cobalt in the valleys of the graphene layer. While experimental studies have shown that the optimum cluster size for Co FT catalysts is 8 – 10 nm because smaller clusters are sintering faster and interact stronger with the metal oxide support [1], this behavior is inhibited by using a corrugated 2D material support as done.

In this work graphene-supported Co clusters are investigated by means of high-resolution X-ray photoelectron spectroscopy (HR-XPS), infrared reflectance absorption spectroscopy (IRRAS) and temperature-programmed desorption (TPD). The Co/Gr/Rh(111) system serves as model catalyst to investigate the properties of Co clusters in regard to available adsorption sites, morphology, thermal stability and to determine the catalytically active sites. To gather this information, CO was used as a probe molecule. The CO adsorption is well studied on clusters (Pt [10], Pd [11], Fe [12], Co [13]) and single crystal surfaces (e.g., Co (0001)) [6,7] which allow us to determine properties of the system investigated in this work. Additionally, the dissociation products of CO were used to determine the influence of carbon and oxygen adatoms on the reactivity of the Co clusters.

2. Methods

2.1. High-resolution XPS

The HR-XPS experiments were performed at the synchrotron facility BESSY II of the Helmholtz-Zentrum Berlin at the UE56/2-PGM2

* Corresponding author.
E-mail address: christian.papp@fu-berlin.de (C. Papp).
[1] These authors contributed equally to this work.

https://doi.org/10.1016/j.susc.2024.122573
Received 16 June 2024; Received in revised form 23 July 2024; Accepted 9 August 2024
Available online 11 August 2024

beamline. Our own transportable UHV apparatus ($p = 1 - 5 \times 10^{-10}$ mbar) was used for the experiments which consists of two connected chambers (preparation and analysis chamber) [14]. The preparation chamber is equipped with a sputter gun for sample cleaning (Ar^+ sputtering followed by annealing to 1200 K) and an electron beam evaporator for Co deposition as well as a quartz crystal microbalance (QCM) for the determination of the metal deposition rate. For sample analysis, a hemispherical photoelectron energy analyzer is connected to the analysis chamber. Furthermore, a three-stage supersonic molecular beam is attached to the analysis chamber which is used in this work for graphene preparation and CO dosing. The sample temperature can be adjusted between 115 and 1200 K by liquid nitrogen cooling and resistive heating. The sample temperature is monitored by K type thermocouples which are spot-welded directly to the Rh(111) crystal. For temperature-programmed XPS (TPXPS), a tungsten filament is mounted at the backside of the sample for sample heating and simultaneously reducing the magnetic field occurring by resistive heating. The heating rate for TPXPS is 0.3 K s^{-1}.

For graphene preparation, chemical vapor deposition of ethene was performed using the molecular beam. Ethene was dosed at a pressure of $\sim 3 \times 10^{-9}$ mbar at a sample temperature of 920 K. After graphene preparation the uniform growth was checked by XPS. Co was deposited upon graphene preparation by electron beam evaporation and the amount was determined by the QCM resulting in a thickness of 2 Å (0.8 ML). According to the atomic radius of Co in comparison to Rh, this is a total coverage of 0.73 ML in regard to the Rh(111) single crystal surface [15]. Since the clusters are mostly located in the pores of the graphene layer (Figure S1), which corresponds to a surface area of 63 ± 5 %, the average Co cluster size is ~ 170 atoms. Considering that the clusters consist of >1 atomic layer, the approximate cluster size is 2 – 4 nm corresponding to the size of the pores [16,17].

All XP spectra were recorded in normal emission to the photoelectron energy analyzer. The photon energies used for the measurements of the Co 3p, C 1s and Rh 3d, and O 1s spectra were 180, 380, and 650 eV, respectively. The resolution of the XP spectra is 190 meV for the Co 3p core level, 220 meV for the C 1s and Rh 3d core level and 340 meV for the O 1s core level. All measured spectra are referenced to the Fermi energy.

To quantify the measured XP spectra, they were fitted with a set of asymmetric Doniach-Šunjić functions convoluted with Gaussian functions followed by comparison of the obtained fit areas with the integrals of data with known coverage. For the carbon coverage this is the pristine graphene layer, which corresponds to a coverage of 1.19 ML due to the lattice mismatch of graphene/Rh(111) of (12 × 12)/(11 × 11) [9]. The oxygen coverage was obtained from the saturated CO layer on the annealed Co clusters where the C coverage is known from comparison to the graphene signals.

2.2. Infrared reflection adsorption spectroscopy

The experiments were performed in an ultrahigh vacuum (UHV) apparatus equipped with a sputter gun, a LEED system (MCP-LEED, Omicron), a quadrupole mass spectrometer (HAL 201, Hiden) with a Feulner-cup for TPD-measurements and a FT-IR spectrometer (Vertex 80v, Bruker) to record IR spectra in grazing reflection geometry. The Rh (111) single crystal (8 × 6 mm, MaTeck) was mounted to a cryostat using a homemade sample holder which has been described in detail elsewhere [18]. The Rh(111) sample was cleaned by sputter and annealing cycles using Ar^+ ion sputtering ($p(Ar) = 1 \times 10^{-6}$ mbar, T = 300 K, E = 2 kV, I = 10 mA, t = 30 min) and subsequent annealing to 1100 K for 10 min. The cycles were repeated until the crystal showed a sharp LEED image expected for the (111) surface.

For the preparation of the graphene layer the sample was heated in a propene atmosphere (2×10^{-8} mbar, Sigma-Aldrich Messer CANGas, 99.5 %) to 970 K for 50 min. The long-range order of the graphene layer was determined by LEED images and possible defects in the graphene layer were determined by the absence of IR signals after CO adsorption.

Co (2 mm rod, MaTeck, 99.95 %) corresponding to a nominal thickness of 2 Å (1 ML with respect to Co(0001)) was evaporated onto the graphene layer using an electron beam evaporator (EFM3, Focus; E = 997 V, I_{Fil} = 1.89 A, I_E = 13.0 mA) with a rate of 2 Å/min as determined by a quartz microbalance.

The CO-IRRA-spectra were taken by accumulating 256 scans with a nominal resolution of 4 cm^{-1} and a zero-filling factor of 16. The sample was exposed to ^{12}CO using a pin-hole doser (pin hole: 50 µm, Plano) with computer controlled pneumatic valves with a resolution of 0.2 s. The pressure in the gas reservoir was controlled by a Baratron (626D, 10 Torr, MKS) and set to 0.33 mbar. Temperature dependent IRRAS was done by annealing the sample to a given temperature (typical heating rate 2 K s^{-1}) and IR spectra were measured subsequently. For annealing temperatures above 180 K, the sample was cooled down to 180 K prior to the IRRAS measurement to limit baseline distortions. TPD spectra were taken using a heating rate of 2 K s^{-1}.

3. Results and discussion

3.1. As-prepared Co clusters

To gather information about the structure of the as-prepared Co nanoclusters, CO was adsorbed while *in situ* high-resolution XPS was performed. The resulting C 1s spectra are shown in Fig. 1. Before CO adsorption, the two graphene features C^1 (285.01 eV) and C^2 (284.42 eV), which are assigned to strong and weak interactions between the graphene layer and the Rh(111) surface, respectively, are present in the C 1s spectra (Fig. 1a) [9,19]. Furthermore, carbide on Rh(111) (C^{Rh}, 283.87 eV) is found, originating from the graphene preparation [19]. During CO adsorption on the as-prepared Co clusters, three CO features are evolving. The first evolving CO contribution at 285.69 eV is assigned to CO adsorbed at on-top sites (Fig. 1a, blue). The second CO peak at lower binding energy side shifts from 285.15 to 285.26 eV with increasing CO exposure and is assigned to CO adsorbed at bridge or hollow sites on the Co clusters (Fig. 1a, red). The shift to higher binding energy during CO adsorption of the CO peak is due to increasing lateral interactions. The assignment of these first two peaks was made according to literature: Binding energies reported for CO adsorbed at on-top sites on Co(0001) were 285.7 – 285.5 eV [6,7,20], and 285.1 – 285.0 eV [7,20] for CO adsorbed at bridge and hollow sites. The binding energies of CO adsorbed at bridge or hollow sites could not be further distinguished. Higher binding energies for the two CO induced features in the XP spectra were reported by Lahtinen *et al.* [5] The reported values were 286.2 and 285.7 eV for CO^{top} and $CO^{bridge/hollow}$, respectively [5]. Nevertheless, the binding energy difference between the two species is similar in these works ($\Delta E = 0.5 \pm 0.1$ eV) and are in agreement with the results from our experiments ($\Delta E = 0.43$ eV). Thus, the higher binding energy component was assigned to CO^{top} and the lower binding energy signal to $CO^{bridge/hollow}$. With increasing CO exposure, a third signal at higher binding energy side of the CO^{top} peak grows. This signal at 285.99 eV is assigned to CO adsorbed at the edges of the clusters. C 1s signals contributing from CO adsorbed at step or edge sites are often observed at lower binding energies than the signals which are assigned to CO adsorbed at on-top sites [10–12,21]. Moreover, adsorption on step sites, e.g., on stepped Pt surfaces or supported Pt clusters is found to be more stable than adsorption at terraces [10,21]. This is different on Co surfaces, where comparison of the adsorption energies of H_2 on the flat Co(0001) surface with the corrugated Co(11–20) and Co (10–12) showed that H_2 adsorption is more stable on Co(0001) than on the lower coordinated surface atoms of Co(11-20) and Co(10-12) [22]. Additionally, IR spectra recorded during CO adsorption on a defective Co surface revealed a feature at higher wavenumbers (2080 cm^{-1}) than the on-top band (2043 cm^{-1}) which is only present at higher CO coverages, that is, when bridge and hollow sites are already occupied and the CO coverage is close to saturation [7]. This is in agreement with our

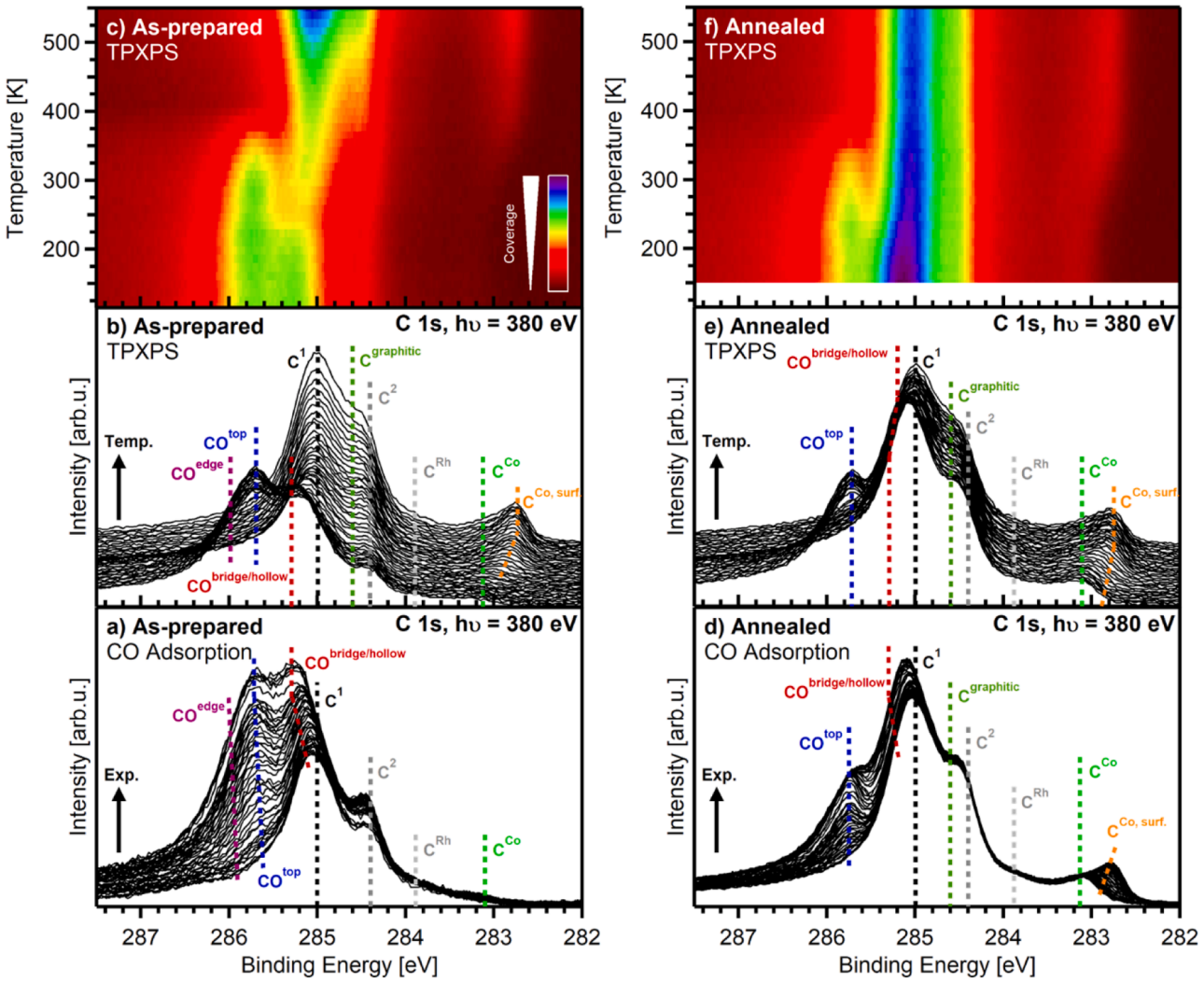

Fig. 1. (a) Spectra of the C 1s core level region (hυ = 380 eV) recorded during CO adsorption on as-prepared Co clusters on Gr/Rh(111), (b) TPXPS of CO adsorbed on as-prepared Co clusters and (c) density plot of the TPXP spectra shown in (b); (d) Spectra of the C 1s core level region (hυ = 380 eV) recorded during CO adsorption on annealed Co clusters on Gr/Rh(111), (e) TPXPS of CO adsorbed on annealed Co clusters and (f) density plot of the TPXP spectra shown in (e). The legend in (c) is also valid for (f).

results where CO^{edge} starts to grow after most of the top and bridge/-hollow sites are already occupied. The binding energies determined in this work and comparison with literature values are listed in Table 1.

The spectra shown in Fig. 1 were fitted and analyzed quantitatively. For the quantitative analysis the peak areas of the distinguishable carbon features were compared to the peak areas of the pristine graphene layer with a known carbon coverage of 1.19 ML, while neglecting possible photoelectron diffraction effects [9]. The data obtained from the quantitative analysis is depicted in Fig. 2. For clarity, only the data of the CO and cobalt carbide features are shown. The quantitative analysis of other observed species is shown in the Supporting Information in Figure S2. Before CO adsorption minor amounts of CO ($\Theta(CO^{top})$ = 0.008 ML) and cobalt carbide ($\Theta(C^{Co}) = 0.006 \pm 0.001$ ML; 283.15 eV) were already present on the Co/Gr/Rh(111) sample. The latter did not show any changes throughout the CO adsorption experiment. C^{Co} was also assigned in agreement with literature [3,6,7]. With increasing CO exposure, CO^{top} and $CO^{bridge/hollow}$ start to increase. CO^{edge} starts to grow at 0.9 L. At 2.05 L CO exposure, CO^{edge}, CO^{top} and $CO^{bridge/hollow}$ reached a coverage of 0.03, 0.11 and 0.12 ML, respectively. To ensure saturation of CO on the cobalt clusters, the CO pressure on the surface was increased to $\sim 2 \times 10^{-7}$ mbar by opening the flag of the molecular beam and directing the CO stream straight to the sample surface. The increased CO pressure leads to a further increase in CO partial coverages: a CO^{edge} coverage of 0.04 ML, CO^{top} of 0.12 ML and $CO^{bridge/hollow}$ of 0.16 ML was reached. Fig. 3a shows the C 1s spectra recorded upon saturation including the corresponding peak fitting. The graphene signals were subtracted from the original spectrum for reasons of clarity.

Table 1
C 1s binding energies of CO at CO saturation coverage on the as-prepared and annealed cobalt clusters and the cobalt carbides measured in this work and corresponding values reported in literature. The binding energies are given in eV. Binding energies determined in this work are referenced to the Fermi energy.

	As-prepared	Annealed	Literature
CO^{edge}	285.99	–	–
CO^{top}	285.69	285.75	285.5 [6]
			285.7 [7,20]
			286.2 [5]
$CO^{bridge/hollow}$	285.26	285.28	285.0 [7]
			285.1 [20]
			285.7 [5]
C^{Co}	283.15	283.13	283.1 [6]
			283.4 [23]
$C^{Co,\ surface}$	282.75	282.77	282.8 [23]
			282.7 [6]

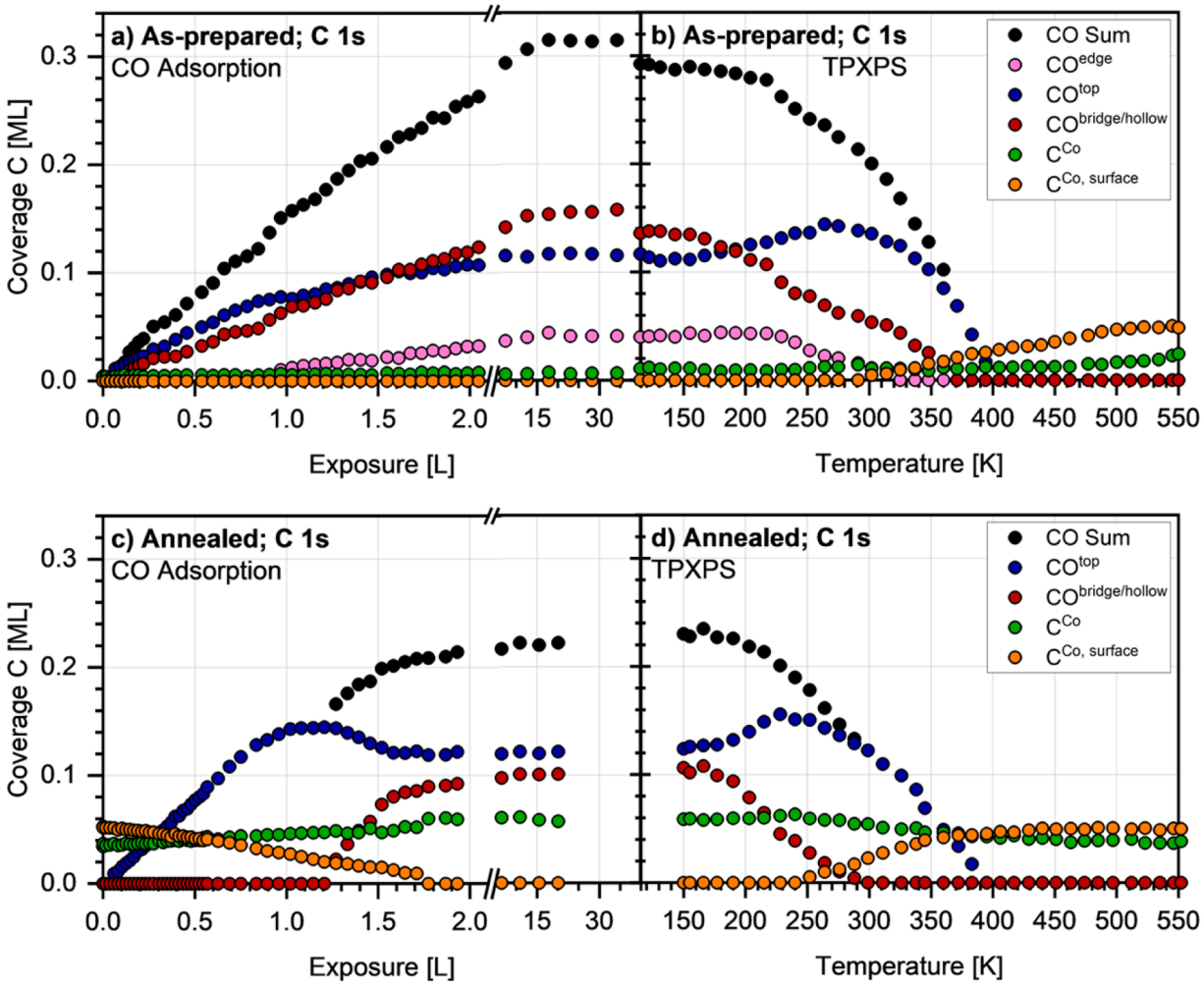

Fig. 2. Quantitative analysis of the (a) C 1s data acquired during CO adsorption on as-prepared Co clusters and (b) TPXPS and (c) C 1s data acquired during CO adsorption on annealed Co clusters and (d) TPXPS.

Please refer to the Supporting Information for the original XP spectra which include all signals (Figure S3). A total CO coverage of 0.32 ML is reached on the as-prepared Co clusters (Fig. 2, black). Only the graphene signals C^1 and C^2 decreased upon CO adsorption due to damping of the emitted photoelectrons by the adsorbed CO layer (Figure S2a). Similar to the graphene signals, the Co 3p signal is also damped upon CO adsorption and shows an additional CO induced doublet with the $3p_{3/2}$ at 59.4 eV and the $3p_{1/2}$ at 60.2 eV, which are at 0.5 eV higher binding energy than the Co $3p_{3/2}$ and Co $3p_{1/2}$ signals, respectively (Figure S5).

We are only able to observe one core level region during the *in situ* experiment. Thus, only one spectrum of the O 1s core level region was recorded before and after the CO adsorption experiment on the as-prepared Co clusters. The O 1s spectrum recorded before the CO adsorption experiment is shown in Figure S6. Originating from the Co evaporation process and residual gas in the chamber, H_2O (533.57 eV, 0.03 ML) and OH (531.31 eV, 0.10 ML) were present on the as-prepared clusters [24]. The formation of OH as a result of dissociative adsorption at defect sites was reported by Weststrate *et al.* [24] on a Co(0001) surface. In our case, the as-prepared clusters possess similar active sites in form of edges and kinks. Thus, dissociative adsorption also leads in our experiment to the presence of OH on the sample. Since we also observe a minor amount of CO before exposing the sample to CO for the first adsorption experiment, a minor amount of CO should also be present in the O 1s spectrum. However, it was not possible to separate this species from the H_2O and OH signals. After the sample was exposed to CO, the spectrum shown in Fig. 3d was recorded. Similar to the C 1s data, it shows two features which are assigned to CO^{top} and $CO^{bridge/-hollow}$, respectively. The binding energy of CO^{top} is 532.28 eV and the $CO^{bridge/hollow}$ binding energy is 531.03 eV. These binding energies are in agreement with literature values obtained for CO on Co(0001) [5,7,20]. Although we assigned the two CO species to CO^{top} and $CO^{bridge/-hollow}$, based on the results in the C1s region we assume the signal of CO on the edges and steps of the clusters to overlap with the other CO species. A similar behavior was found on supported Pt nanoclusters [10]. The O 1s binding energies of the CO and cobalt oxide features measured in this experiment are listed in Table 2. From the quantitative analysis, the amount of CO^{top} is determined to be 0.25 ML while the amount of $CO^{bridge/hollow}$ is 0.21 ML. This is a total coverage of 0.46 ML which is higher than the coverage obtained from the C 1s data. But before CO adsorption, 0.13 ML of H_2O and OH were present on the sample. Subtracting this amount from the amount determined from the O 1s spectrum recorded after CO exposure of the sample results in a total CO coverage of 0.33 ML. From the C 1s data a value of 0.32 ML was determined. Thus, the result from the O 1s data fits the values obtained from the C 1s data within the experimental error (± 10 %).

CO adsorption on as-prepared Co clusters was also investigated using IRRAS. Fig. 4a shows IRRA-spectra recorded after saturating Co clusters deposited at 115 K with CO on a graphene layer on Rh(111). The black spectrum was obtained after CO adsorption on the as-prepared Co clusters. The spectrum is dominated by an asymmetric signal at 2071 cm^{-1} with a shoulder on the low-energy side extending down to 2000 cm^{-1}. A second signal is observed at 1895 cm^{-1}. The IR-signals/shoulder

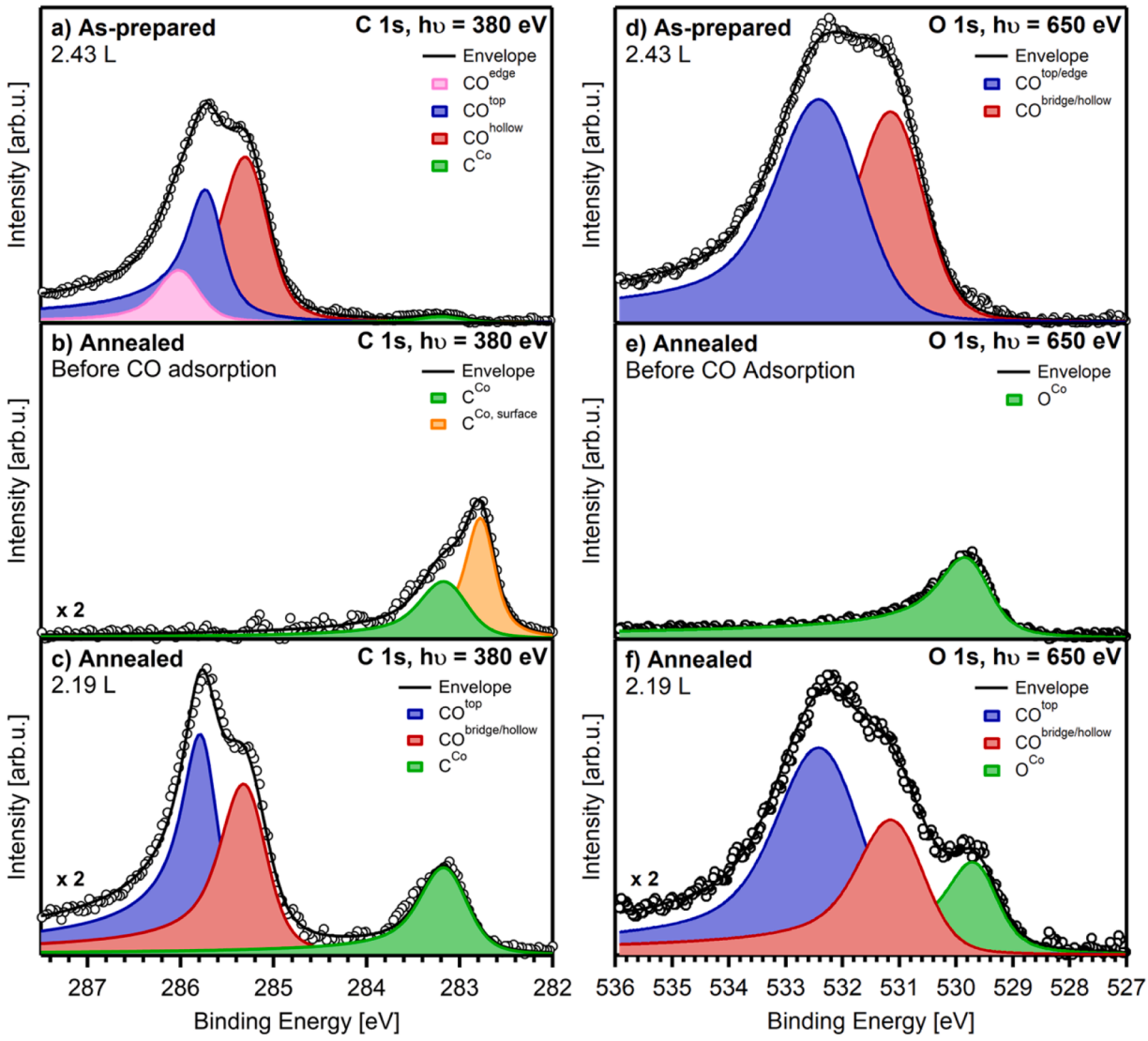

Fig. 3. (a) XP spectra of the C 1s core level region acquired after CO adsorption on the as-prepared Co clusters on Gr/Rh(111), (b) after TPXPS ($T_{s,\ max}$ = 550 K), and (c) after CO adsorption on the annealed Co clusters. (a) – (c) show the C 1s XP spectra including fits after subtracting the graphene signals. Please refer to the Supporting Information for the original spectra including the fits of the graphene substrate. (d) XP spectra of the O 1s core level region obtained after CO adsorption on the as-prepared Co clusters on Gr/Rh(111), (e) after TPXPS ($T_{s,\ max}$ = 550 K), and (f) after the CO adsorption on the annealed Co clusters.

Table 2
O 1s binding energies of CO on the as-prepared and annealed cobalt clusters and the cobalt carbides measured in this work and corresponding values reported in literature. The binding energies are given in eV. Binding energies determined in this work are referenced to the Fermi energy.

	As-prepared	Annealed	Literature
CO^{top}	532.28	532.28	531.3 [6]
			532.1 [7]
$CO^{bridge/hollow}$	531.03	531.03	530.7 [7]
O^{Co}	529.73	529.71	529.3 [6]

above 1950 cm^{-1} are in line with the IRRA spectra observed on Co clusters deposited on epitaxial alumina films [25]. Those signals are assigned to CO bound at on-top sites. CO saturation coverage on Co (0001) showed a signal at 2057 cm^{-1} with a shoulder around 2034 cm^{-1} that was assigned to CO adsorption on the on-top sites of the surface [7]. It should be noted, that the signal assigned to CO on-top sites observed at saturation coverage is due to at least two different signals as becomes clear by looking at the adsorption series (Figure S7). To this end, the IRRA spectra are well in line with the XPS results discussed above indicating the presence of on-top bound CO at different sites. On other low index surfaces, CO was also found to bind preferentially at on-top sites and comparable stretching frequencies were observed [7]. The signals are typically found to be blue-shifted with increasing coverage suggesting a significant dipolar interaction between the adsorbates. The position and width of the IR signals were also found to depend on the preparation conditions i.e. temperature, the pressure of CO but also the presence of defects or impurities such as carbon or oxygen atoms [7,20,26]. On Co(0001) additional peaks at lower wavenumbers are found at saturation. The peak observed at 1862 cm^{-1} was assigned to CO adsorption on hollow sites, while a signal at 1908 cm^{-1} observed at medium coverage was assigned to adsorption on bridge sites [7]. However, it should be noted that such an assignment solely based on IR spectra is not possible as the frequency range of bridge and hollow sited bound CO are overlapping which has been the source of controversies [27]. Therefore, an assignment of the IRRAS signal of the Co clusters around 1900 cm^{-1} remains ambiguous. However, based on the results from the Co(0001) single crystal, bridge bonded CO is the more likely adsorption site of CO on the Co clusters for the signal at 1895 cm^{-1}. The wavenumbers and their assignment to possible adsorption sites are listed

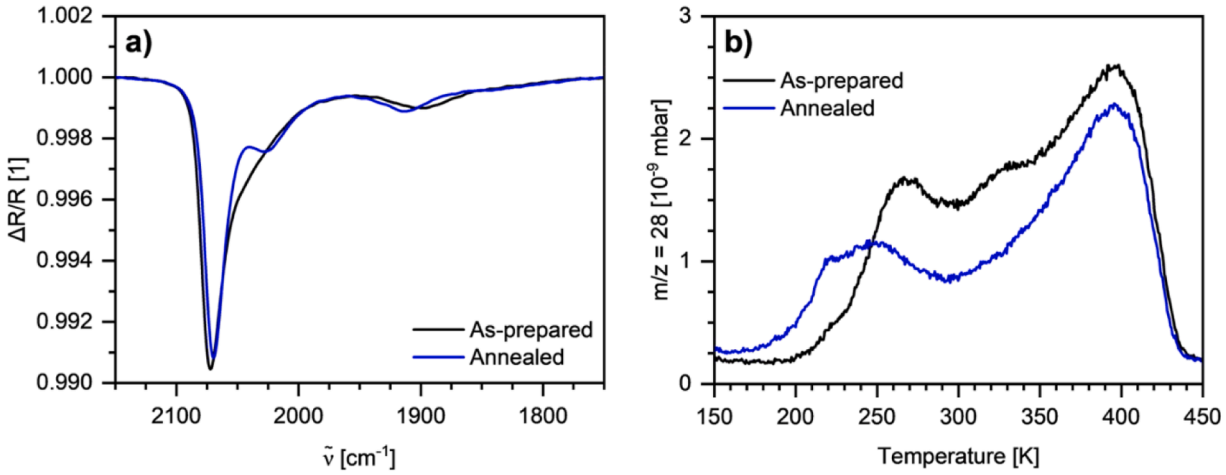

Fig. 4. (a) CO-IRRA spectra taken at 115 K after CO adsorption on the as-prepared Co cluster (black) and after CO adsorption on Co clusters upon saturation with CO and annealing to 450 K (blue). (b) TPD-spectra of the desorption of CO from the as-prepared Co clusters (black) and from the annealed Co clusters (blue).

in Table 3. Thus, in agreement with XPS and literature, we can assign the band/shoulder at higher wavenumbers to CO adsorbed at on-top sites of the clusters and the feature at lower wavenumbers to CO adsorption at bridge or hollow sites. Neither XPS nor IRRAS were able to unambiguously assign either adsorption in bridge or hollow sites. While the IRRA spectra taken during the adsorption series clearly indicate the presence of at least two on-top bound species which cannot be clearly distinguished at saturation coverage due to dipolar interaction, the XPS results provide clear evidence for a third feature which we assigned to CO adsorption at the edges of the clusters.

After CO adsorption the sample was heated to 550 K. The XP spectra recorded during TPXPS are shown in Fig. 1b and the quantitative analysis in Fig. 2b. The $CO^{bridge/hollow}$ coverage is less than after the adsorption experiment due to desorption from the intense x-ray beam from the synchrotron. The areas of the three CO peaks stay constant up to 150 K. By increasing the temperature from 150 to 220 K, the intensity of the CO^{top} species increases while $CO^{bridge/hollow}$ decreases. The coverage of CO^{edge} does not change in this temperature range. From Figure S4 it can be derived that the total CO coverage stays constant during this change in adsorption sites. However, it is possible that due to the desorption of H_2O or OH at ~160 K [24], which were present before the CO adsorption experiment (Figure S6), the adsorbates now distribute in a different way over the surface after additional adsorption sites are available. With increasing temperature, the $CO^{bridge/hollow}$ feature decreases further and also CO^{edge} starts to decrease. CO^{top} stays constant at 0.20 ML up to 300 K. Upon annealing to 300 K, CO^{edge} vanishes and CO^{top} eventually starts to decrease. Simultaneously, a new feature evolves at the lower binding energy side of C^{Co} and is assigned to cobalt carbide located at the surface of the clusters ($C^{Co,\ surface}$; Figs. 1b and Fig. 2b, orange). It is a result of CO dissociation. A carbide at the surface and the respective surface core level shift (SCLS) is also found for iron carbide on Fe clusters on *h*-BN/Rh(111) upon CO dissociation as well as for carbides on Mo(110) [12,28]. CO dissociation is reported to occur at 330 K on defective Co surfaces or on edges and steps of the clusters in our case [6]. $C^{Co,\ surface}$ evolves at a binding energy of 282.95 eV and shifts to lower binding energy with increasing temperature and coverage (Fig. 1b). The final binding energy of $C^{Co,\ surface}$ is 282.75 eV. The binding energy of 282.75 eV for the $C^{Co,\ surface}$ peak fits reported binding energies for surface carbides on Co surfaces [6,23]. A second new feature also starts to evolve at 300 K, which is assigned to graphitic carbon on the cobalt clusters ($C^{graphitic}$, Figure S2b, olive). $C^{graphitic}$ grows at a binding energy of 284.57 eV which is 1.82 eV higher than $C^{Co,\ surface}$ and 1.42 eV higher than C^{Co}. The formation of graphitic carbon upon annealing was also observed by Nakamura *et al.* [3] at a C 1s binding energy of 284.8 eV which is 1.7 eV higher than the binding energy of cobalt carbide. On Fe clusters, the formation of graphitic carbon was also observed, resulting in a binding energy which is 1.93 and 1.46 eV higher than the surface carbide and iron carbide species, respectively [12]. At ~ 480 K, C^{Co} also starts to increase slightly. $C^{Co,\ surface}$ reaches its maximum of 0.05 ML at 500 K while C^{Co} keeps increasing up to 550 K to a maximum coverage of 0.03 ML. The small further increase of C^{Co} is due to restructuring of the clusters [12]. Additionally, the substrate signals C^1 and C^2 of the graphene layer and the Rh 3d signal are increasing as a result of CO desorption and cluster restructuring (Figure S2 and S8) [29]. Restructuring of the clusters changes the shape of the clusters to a more 3D shape. Moreover, Figure S2b shows that the intensity of the C^1 signal increases strongly which is assigned to a higher mobility of the clusters at elevated temperatures leading to agglomeration of the clusters. Thus, the emitted photoelectrons from the underlaying graphene layer are less damped and the signals become more intense. Due to CO dissociation, a cobalt oxide peak (O^{Co}, 0.11 ML, 529.73 eV) is also observed in the O 1s spectrum measured after the TPXPS experiment (Fig. 3e).

The CO desorption was also investigated by TPD measurements (Fig. 4b). The obtained TPD spectrum of the as-prepared Co clusters is very comparable to TPD from pristine Co clusters deposited on epitaxial alumina-films grown on NiAl(110) [25]. In particular, the position of the high-temperature maximum close to 400 K and the low-temperature maximum around 260 K are observed on this system too, indicating that the CO adsorption strength depends only slightly on the support being used. Additionally, the CO TPD of the as-prepared Co clusters shows a peak at 320 K. Comparison to low index surfaces of Co single crystals reveals a strong similarity to the CO TPD spectrum from the reconstructed Co(11–20) surface [30]. The TPD from this surface shows the largest desorption peak slightly below 400 K and a less intense structure around 270 K. A dominant desorption around 400 K and a smaller signal around 320 K is also observed for CO TPD on Co(10–10) [31]. The CO TPD spectrum from the Co(0001) surface also shows the largest desorption between 380 and 400 K but the spectrum is considerably more complex [20]. It exhibits a pronounced narrow peak around

Table 3
Wavenumbers of CO on the as-prepared and annealed cobalt clusters measured in this work and corresponding values reported in literature.

	As-prepared	Annealed	Literature
CO^{top}	2071	2068	2057 [7,25]
	~ 2000	2025	2034 [7,25]
$CO^{bridge/hollow}$	1895	1913	1862 (hollow) [7]
			1908 (bridge) [7]

240 K which has no counterpart in the TPD of the Co clusters. Furthermore, there is a dedicated feature around 300 K and the main peak exhibits a discernable fine structure neither of which is observed for the clusters. It is interesting to note that a defective Co(0001) surface loses all CO desorption features except the high temperature peak (which loses its fine structure) indicating that the complex TPD signatures of the well-ordered Co(0001) surface is governed by the complex rearrangements of CO molecules upon reduction of the coverage due to the strong repulsive interaction between the CO molecules [7]. A comparison of the TPD data to the previously discussed XPS measurements allow the assignment of the desorption maxima to the individual CO adsorption sites. The first desorption maximum (260 K) in the TPD spectrum is attributed to CO desorption from bridge/hollow sites, the second maximum (320 K) to CO desorption from edge sites and the third one (400 K) to desorption from top sites (Table 4). The discrepancies in the desorption temperatures arise from the different procedures by which the desorption temperatures were determined. While the desorption temperatures determined by TPD were determined by the maximum of the corresponding desorption peak, for XPS and IRRAS the temperatures were used at which the signals vanish.

More details into the behavior of CO on the Co clusters are obtained from the IRRAS annealing series shown in Fig. 5a. Upon annealing the as-prepared Co clusters to 175 K, the main signal at 2071 cm^{-1} is reduced in intensity going along with a slight red shift of the signal. Between 180 and 240 K, the signal height remains almost constant, but the signal is significantly red-shifted particularly above 210 K. The signal exhibits an almost linear dependence of the red-shift with temperature and disappears after annealing above 400 K with a final signal position of ~1950 cm^{-1}. The signal height increases significantly when heating from 240 to 320 K (Figure S9a) and further decreases rapidly above 350 K. A similar increase of the CO^{top} intensity is also observed in the XP spectra in the same temperature range (240 - 320 K) indicating a reordering of the CO molecules on the surface, thereby changing the dipole interactions that lead to the observed red shift in the IRRAS data. The signal at around 1900 cm^{-1} exhibits a constant position (white line in Fig. 5a) and an almost linear decay of the signal intensity with temperature (inset in Fig. 5a) resulting in a loss of the signal at 270 K. However, the signal intensity is not zero at this temperature as shown in the inset in Fig. 5a. The $CO^{bridge/hollow}$ signal vanishes as a feature at higher wavenumbers is evolving. Along with $CO^{bridge/hollow}$, this new feature results in a shoulder at lower wavenumbers than the CO^{top} signals (Figure S9). This shoulder starts to vanish only at $T > 300$ K. The total carbon coverage also decreases in the XPS data when the sample is heated from 220 to 270 K by 0.05 ML (Fig. 2 and Figure S4). In this temperature range, rearrangement of $CO^{bridge/hollow}$ to CO^{top} is observable in the XPS data. However, since the CO^{top} signal only increases by 0.01 ML but $CO^{bridge/hollow}$ decreases by 0.05 ML, 0.04 ML of $CO^{bridge/hollow}$ desorbs in this temperature range according to the peak intensities acquired from the XP spectra. CO^{edge} also starts to desorb at 230 K but only decreases by 0.02 ML upon annealing to 270 K and vanishes completely at 325 K. Thus, most of the desorption taking place at temperatures below 270 K can be assigned to desorption of $CO^{bridge/hollow}$. In conclusion, XPS and IRRAS show reorganization at temperatures below 300 K and the partial desorption of $CO^{bridge/hollow}$ is observed in XPS in agreement with the first desorption maximum at $T < 300$ K in the TPD spectrum. The inconsistency between the desorption temperature listed in Table 4 are due to the fact that the XPS $CO^{bridge/hollow}$ temperature is determined from the vanishing of the signal while the IRRAS temperature gives the temperature at which the $CO^{bridge/hollow}$ signal is not distinguishable from the shoulder/background anymore.

3.2. Annealed (C- and O-precovered) Co clusters

The annealed Co clusters are covered with carbon and oxygen from CO dissociation, which offers the possibility to investigate CO adsorption on annealed, C- and O-covered Co clusters. By XPS, four CO adsorption and TPXPS experiments on the annealed and C- and O-covered clusters were performed and the C 1s and O 1s spectra taken at CO saturation coverage for each adsorption and annealing cycle are shown in Figure S10 in the Supporting Information, showing similar results in all cases. The data shown in this section was acquired during the third adsorption and annealing cycle (Figure S10) which was followed *in situ* in the C 1s core level region. The XP spectra of this CO adsorption experiment are shown in Fig. 1d. The first spectrum recorded prior to CO exposure is similar to the spectrum shown in Fig. 3b or Figure S3b. When the sample is exposed to CO, the CO^{top} signal starts to increase first which can be followed in the quantitative analysis shown in Fig. 2c (blue). In this CO adsorption experiment the binding energy of CO^{top} stays constant at 285.75 eV. At the same time, $C^{Co,\ surface}$ decreases while C^{Co} slightly increases (Fig. 2c, orange and green). This is attributed to the population of the surface with CO molecules. Thereby, the surface core level shift vanishes [12,28]. The binding energy of the surface feature shifts to higher values with increasing CO coverage until it is finally similar to the binding energy of C^{Co} (Fig. 1d). Thus, the signal of C^{Co} is increasing during CO adsorption at the expense of $C^{Co,\ surface}$. Please note that the decrease of $C^{Co,\ surface}$ and the increase of C^{Co} should be equivalent, but the intensity of C^{Co} is damped by the adsorbed CO. At 1.02 L, CO^{top} reaches a maximum coverage of 0.14 ML which is 0.04 ML smaller than the CO^{top} coverage on the as-prepared Co clusters. The intensity of CO^{top} stays constant up to 1.21 L. At 1.27 L, $CO^{bridge/hollow}$ starts to grow at a binding energy of 285.19 eV while CO^{top} decreases. The same change in adsorption sites with increasing CO coverage was already reported by Weststrate *et al.* [7] for CO adsorption on Co(0001). $C^{Co,\ surface}$ vanishes completely at an exposure of 1.77 L and C^{Co} reaches its maximum coverage of 0.06 ML. Please note, the total carbide coverage is now less ($\theta(C^{Co} + C^{Co,\ surface}) = 0.06$ ML) than in the beginning of the CO adsorption experiment on the precovered clusters ($\theta(C^{Co} + C^{Co,\ surface}) = 0.09$ ML). This is again due to damping of the carbide by the adsorbed CO layer while the actual carbide amount present on the clusters is not affected. At higher CO exposures, CO^{top} decreases to 0.12 ML while $CO^{bridge/hollow}$ increases to 0.10 ML and reaches its final binding energy of 285.28 eV. Fig. 3c depicts the spectrum recorded after CO adsorption including the fitted peaks. In this adsorption experiment on the annealed clusters, no CO adsorption at edges of the clusters was observed. Thus, we conclude that these sites are now blocked for the adsorption of CO by carbon and oxygen. The CO saturation coverage in this experiment is 0.22 ML which is 0.10 ML (= 30 %) less than in the adsorption experiment on the as-prepared clusters. This again supports the assumption that adsorption sites are blocked by the dissociation products of the first CO adsorption experiment. The O 1s

Table 4
Desorption temperature of CO on as-prepared and annealed Co clusters as determined by the XPS, IRRAS and TPD measurements. The temperatures are given in K. The XPS and IRRAS temperatures are determined by the temperatures where the corresponding species vanishes while the TPD temperature corresponds to the desorption maximum in the spectra.

	As-prepared			Annealed			Literature
	XPS	IRRAS	TPD	XPS	IRRAS	TPD	
CO^{top}	400	400	400	400	400	400	400 [7,25]
CO^{edge}	325	–	320	–	–	–	320 [30,31]
$CO^{bridge/hollow}$	370	270	260	300	270	220 - 250	240 - 250 [7] 260 [25]

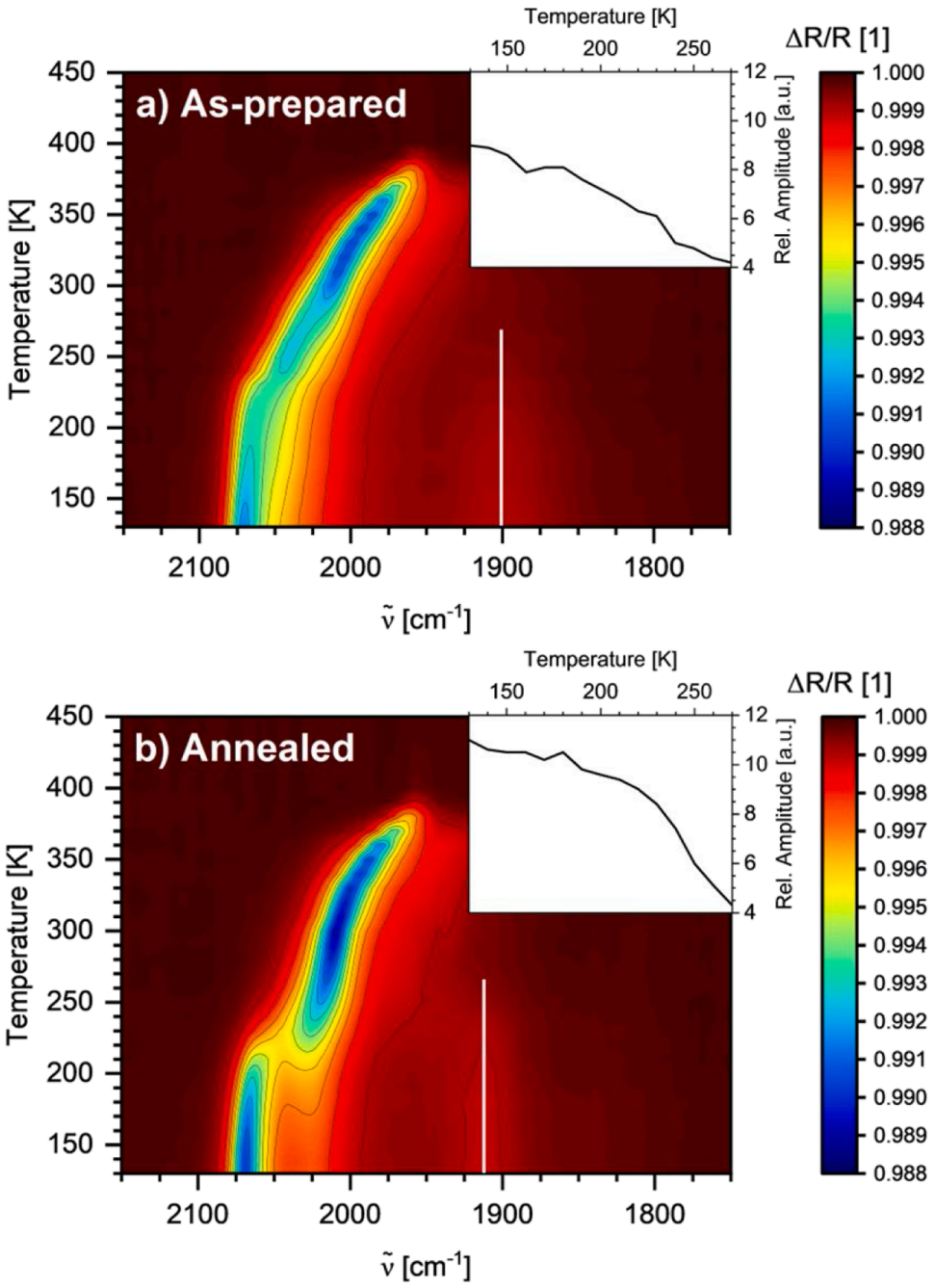

Fig. 5. IRRAS annealing series of CO adsorbed on Co particles. The particles were heated to the temperature given on the y-axis before the IR spectra were taken. (a) Annealing series of CO adsorbed on as-prepared Co clusters (corresponding to the black IRRA spectrum and black TPD in Fig. 4). The inset shows the evolution of the signal intensity marked in (a) by the white line. (b) annealing series of CO adsorbed on annealed Co clusters (corresponding to the blue IRRA spectrum and blue TPD in Fig. 4). The inset shows the evolution of the signal intensity marked in (b) by the white line.

spectrum measured after the CO adsorption experiment is shown in Fig. 3f. The oxygen coverage determined from the fits is 0.14 ML for CO^{top} and 0.08 ML for $CO^{bridge/hollow}$. Thus, the total CO coverage is also 0.22 ML as determined from the C 1s data. However, the distribution between the components is slightly different which is attributed to the uncertainties in the experiment and the analysis of the data. Same as the cobalt carbide, the cobalt oxide peak decreases during the CO adsorption experiment from 0.11 to 0.06 ML due to damping of the emitted photoelectrons by the adsorbed CO. However, while $C^{Co,\ surface}$ shifts to higher binding energy during CO adsorption, O^{Co} shifts to lower binding energy from 529.73 to 529.59 eV.

In comparison to the XPS data, where the number of distinguishable CO features decreases from three signals (CO^{edge}, CO^{top}, $CO^{bridge/hollow}$) for the as-prepared clusters to two signals (CO^{top}, CO^{bridge}) for the annealed/precovered clusters, the IRRA spectrum (blue, Fig. 4a), which was taken after exposing the annealed clusters to CO until saturation, shows no distinct changes. The most prominent change upon annealing is the development of a well-defined signal around 2025 cm^{-1} replacing the low-energy shoulder of the signal observed for the as-prepared clusters (Fig. 4a). Furthermore, the maximum of the most intense signal is slightly red-shifted and now observed at 2068 cm^{-1}. The peak at lower wavenumbers assigned to CO adsorbed at bridge or hollow sites exhibits a smaller linewidth and is blue shifted to 1913 cm^{-1}. An integration of the IR spectra revealed that the first annealing results in a

reduction of the IR intensity by 10 % indicating adsorption side blocking as also determined from the XPS data. With respect to the smaller decrease of IR intensity as compared to that observed by XPS it is important to keep in mind that annealing of the particles will lead to restructuring/sintering both of which can change the CO adsorption properties. Due to the metal surface selection rule changes in adsorption geometry with respect to the surface will impact signal intensity. The latter can also be altered by changes in electronic and dynamic coupling of the CO molecules. Hence, IR intensity is not expected to compare quantitatively with the XPS result.

After reaching CO saturation on the C- and O-covered Co clusters, temperature-programmed XPS was performed. The quantitative analysis of the C 1s data is shown in Fig. 2d. Since the sample temperature in the CO adsorption experiment on the annealed clusters was 35 K higher (T_S = 150 K) than in the first adsorption experiment (T_S = 115 K), the TPXPS also starts at 150 K. Yet, no changes in the spectra were observed when the sample was heated to 170 K. Further increase of the temperature leads to the desorption of $CO^{bridge/hollow}$ while CO^{top} starts to increase due to a change in adsorption sites. Fig. 2d shows that indeed the total CO coverage decreases at $T > 170$ K and not all of the CO molecules adsorbed at bridge/hollow sites change to on-top adsorption sites. At 228 K, CO^{top} reaches a maximum of 0.15 ML which is similar to the maximum CO^{top} coverage during CO adsorption. CO^{top} starts to decrease at $T > 260$ K. Simultaneously, $C^{Co,\ surface}$ reemerges and C^{Co} starts to decrease. $CO^{bridge/hollow}$ vanishes completely at 290 K while CO^{top} and C^{Co} keep decreasing and $C^{Co,\ surface}$ increases. During the reappearance of $C^{Co,\ surface}$, it shifts to lower binding energy until it reaches its initial binding energy of 282.77 eV. At 395 K, all CO has desorbed from the Co clusters. At the same temperature, C^{Co} and $C^{Co,\ surface}$ reach a similar coverage as in the beginning of the CO adsorption experiment of 0.04 and 0.05 ML, respectively. By annealing the sample to 550 K no further changes are observed. All other features in the C 1s core level region (C^1, C^2, C^{Rh}, $C^{graphitic}$) do not change throughout the CO adsorption and TPXPS experiments on the annealed clusters (Figure S2c and S2d). In this temperature-programmed experiment of the annealed Co clusters, no CO dissociation occurs because the carbide and oxide coverages are similar before and after the experiments. This indicates that the active sites – that is the edges of the clusters – are blocked by carbon and oxygen adatoms or have vanished completely upon restructuring and agglomeration of the Co clusters. As discussed before, cluster ripening/restructuring results in the clusters adapting a more 3D structure. Hence, the available adsorption sites on the clusters' surface are altered as well, which can also lead to the disappearance of active sites for CO dissociation upon annealing. Such passivation of the catalytic activity of nanoclusters was also found for Fe clusters on *h*-BN/Rh(111) [12].

TPD measurement was also performed upon CO adsorption on the annealed Co clusters. In comparison to CO desorption from the as-prepared Co clusters (black, Fig. 4b), the integral intensity decreases by 23 % for the annealed Co clusters (blue, Fig. 4b), similar to the reduction found in XPS of 30 %. Apart from the reduction of the integral intensity, the first annealing also alters the shape of the desorption spectrum. In particular, the low-temperature desorption feature of the as-prepared clusters at 270 K is shifted to lower temperature exhibiting a first maximum at 220 K for the annealed clusters. The maximum is rather broad and extents up to 250 K. A shift to lower temperature for $CO^{bridge/hollow}$ desorption is also observed in the XPS data. $CO^{bridge/hollow}$ vanishes at 300 K which is a 70 K lower temperature than observed for the as-prepared clusters (370 K). While the desorption of the as-prepared clusters shows a peak at 320 K, this feature is lost for subsequent TPD spectra. It should be noted that the CO TPD spectrum from the unreconstructed Co(11-20) surface exhibits a small peak around 320 K which is depleted upon CO induced reconstruction of the surface [30]. Concomitantly, the reconstruction leads to the appearance of the above mentioned low-temperature peaks in the TPD spectra, which is qualitatively like the effect observed for the clusters upon annealing. The most intense peak is again found around 400 K, only its intensity drops after the first annealing. With respect to the most strongly bound CO, the TPD spectra reveal no significant change of the binding strength but some reduction in intensity indicating a loss of these adsorption sites. The XPS data also shows no significant change in binding strength of the most strongly bound CO feature (CO^{top}). For the as-prepared and annealed clusters, CO^{top} vanishes completely at 400 K in both experiments in agreement with the TPD results.

The annealed Co clusters were also investigated by IRRAS after exposure to CO. The second IRRAS annealing series of the sample is shown in Fig. 5b (and Figure S9b) and reveal some changes. Firstly, the main signal around 2070 cm^{-1} is stable up to about 180 K and disappears at about 230 K. Concomitant to this decrease, the signal at 2030 cm^{-1} increases in intensity and both signals are shifted to lower wavenumbers. Qualitatively, the development of the latter signal is similar to that observed for the as-prepared clusters, however, the red-shift deviates from a simple linear correlation and the increase in signal intensity at intermediate temperatures (260 - 350 K) is even more pronounced than for the as-prepared clusters, similar to the XPS data. Moreover, the rapid decrease of the signal intensity above 350 K is very comparable in both cases mirroring the similarity of the TPD spectra and TPXPS data at high temperatures. The signal height of the bridge bonded CO molecules decreases monotonically. Contrary to the as-prepared Co clusters which show a linear decrease of the intensity, the signal of the annealed sample decreases only by about 25 % up to 220 K and disappears at 270 K. It should be noted though, that IR intensity remains in the range compatible with bridge/hollow bonded CO at higher temperature. However, the spectra do not show a distinct signal anymore, which renders the quantification of this signal difficult. The desorption curve of $CO^{bridge/hollow}$ is also steeper for the annealed clusters in the XPS data (Fig. 2). Desorption of $CO^{bridge/hollow}$ starts at 200 K and the species vanished completely at 300 K. The investigations on Co single crystal surfaces have shown that the thermal desorption of CO as well as the IR signals are strongly altered by the presence of defects or impurities on the surface. The latter is particularly important as CO dissociation was shown in the XPS data to occur in agreement with findings for the low index Co single crystal surface at elevated temperatures. With respect to the Co clusters, it is expected that growth of the Co clusters at low temperature will result in clusters not adopting the thermodynamic equilibrium shape. As shown by an additional annealing series on Co particles annealed prior to CO adsorption (Figure S14), the observed effects for the different annealing series result from a combination of thermally induced restructuring of the clusters and decomposition of CO and the corresponding impurity formation, which have also been observed by XPS.

After the first annealing cycle the adsorption properties of the clusters remain stable as the IRRAS and XPS results for subsequent adsorption/annealing series are very similar (see Supporting Information). Annealing to higher temperatures of up to 1100 K shows a further agglomeration of the particles and subsequently the intercalation of Co (see Supporting Information).

4. Conclusion

Graphene-supported Co clusters were investigated in this work by XPS, IRRAS and TPD. CO was used as probe molecule to determine the available adsorption sites on the Co clusters. The XPS measurements revealed CO adsorption at edge, on-top and bridge/hollow sites on the as-prepared Co clusters. The existence of three different adsorption sites were confirmed by the TPD measurements with maxima at 260, 320 and 400 K for $CO^{bridge/hollow}$, CO^{edge} and CO^{top}, respectively. Upon annealing the sample to 450 K (TPD, IRRAS)/550 K (XPS), CO dissociation and cluster restructuring was observed. Due to the dissociation of CO, the clusters become covered with carbon and oxygen adatoms. For the evolving cobalt carbide, a surface core level shift was observed in the C 1s core level spectra which vanishes after CO adsorption. Further CO adsorption experiments on the annealed/precovered clusters showed a

decrease in the amount of CO adsorbed on the clusters for all applied methods due to site blocking by the adatoms. Thus, no adsorption at edge sites was observed. On the precovered clusters no further CO dissociation was observed. We conclude that the carbon and oxygen adatoms are blocking the active sites on the clusters for CO dissociation and determine the active sites as the edges and kinks of the clusters.

We showed in this work, that the use of different spectroscopic techniques is necessary to gain an overall understanding of such system, while IRRAS revealed changes in dipolar coupling during reorganization of the CO molecules, TPD was used to determine the desorption temperatures in a precise manner and XPS revealed quantitatively the population of the adsorption sites during CO exposure and the impurities upon CO decomposition. All information considered, we have gained a comprehensive understanding of the as-prepared and annealed/C- and O-precovered Co/graphene/Rh(111) system.

CRediT authorship contribution statement

Natalie J. Waleska-Wellnhofer: Conceptualization, Visualization, Validation, Formal analysis, Investigation, Data curation, Writing – original draft, Writing – review & editing. **Sophie Arzig:** Writing – review & editing, Writing – original draft, Investigation, Formal analysis, Data curation. **Fabian Düll:** Investigation, Data curation. **Udo Bauer:** Investigation, Data curation. **Phiona Bachmann:** Investigation, Data curation. **Johann Steinhauer:** Investigation, Data curation. **Christian Papp:** Writing – review & editing, Supervision, Resources, Project administration, Funding acquisition, Conceptualization. **Thomas Risse:** Writing – review & editing, Validation, Supervision, Resources, Project administration, Funding acquisition, Conceptualization.

Declaration of competing interest

The authors declare that they have no known competing financial interests or personal relationships that could have appeared to influence the work reported in this paper.

Data availability

The data underlying this study is available at 10.5281/zenodo.11654358.

Acknowledgements

C. Papp and coworkers thank Helmholtz-Zentrum Berlin for allocation of synchrotron-radiation beamtime and BESSY II staff for support during beamtime. This work was funded by the Deutsche Forschungsgemeinschaft within SFB 953 “Synthetic Carbon Allotropes” (Project No 182849149) and within the Heisenberg program (Project No 493259940).

Supplementary materials

Supplementary material associated with this article can be found, in the online version, at doi:10.1016/j.susc.2024.122573.

References

[1] J. van de Loosdrecht, F.G. Botes, I.M. Ciobica, A. Ferreira, P. Gibson, D.J. Moodley, A.M. Saib, J.L. Visagie, C.J. Weststrate, J.W. Niemantsverdriet, Fischer–Tropsch Synthesis: catalysts and Chemistry, in: Compr. Inorg. Chem. II, Elsevier, 2013, pp. 525–557, https://doi.org/10.1016/B978-0-08-097774-4.00729-4.

[2] F. Greuter, D. Heskett, E.W. Plummer, H.J. Freund, Chemisorption of CO on Co (0001). Structure and electronic properties, Phys. Rev. B 27 (1983) 7117–7135, https://doi.org/10.1103/PhysRevB.27.7117.

[3] J. Nakamura, I. Toyoshima, K. Tanaka, Formation of carbidic and graphite carbon from CO on polycrystalline cobalt, Surf. Sci. 201 (1988) 185–194, https://doi.org/10.1016/0039-6028(88)90605-X.

[4] J. Lahtinen, J. Vaari, A. Taio, A. Vehanen, P. Hautojärvi, Adsorption and desorption measurements of CO and O2 on cobalt, Vacuum 41 (1990) 112–114, https://doi.org/10.1016/0042-207X(90)90289-B.

[5] J. Lahtinen, J. Vaari, K. Kauraala, Adsorption and structure dependent desorption of CO on Co(0001), Surf. Sci. 418 (1998) 502–510, https://doi.org/10.1016/S0039-6028(98)00711-0.

[6] C.J. Weststrate, P. van Helden, J. van de Loosdrecht, J.W. Niemantsverdriet, Elementary steps in Fischer-Tropsch synthesis: CO bond scission, CO oxidation and surface carbiding on Co(0001), Surf. Sci. 648 (2016) 60–66, https://doi.org/10.1016/j.susc.2015.10.050.

[7] C.J. Weststrate, J. van de Loosdrecht, J.W. Niemantsverdriet, Spectroscopic insights into cobalt-catalyzed Fischer-Tropsch synthesis: a review of the carbon monoxide interaction with single crystalline surfaces of cobalt, J. Catal. 342 (2016) 1–16, https://doi.org/10.1016/j.jcat.2016.07.010.

[8] C. Papp, From flat surfaces to nanoparticles: in situ studies of the reactivity of model catalysts, Catal. Letters 147 (2017) 2–19, https://doi.org/10.1007/s10562-016-1925-0.

[9] A.B. Preobrajenski, M.L. Ng, A.S. Vinogradov, N. Mårtensson, Controlling graphene corrugation on lattice-mismatched substrates, Phys. Rev. B 78 (2008) 073401, https://doi.org/10.1103/PhysRevB.78.073401.

[10] K. Gotterbarm, F. Späth, U. Bauer, C. Bronnbauer, H.-P. Steinrück, C. Papp, Reactivity of graphene-supported Pt nanocluster arrays, ACS Catal 5 (2015) 2397–2403, https://doi.org/10.1021/acscatal.5b00245.

[11] K. Gotterbarm, C. Bronnbauer, U. Bauer, C. Papp, H.-P. Steinrück, Graphene-supported Pd nanoclusters probed by carbon monoxide adsorption, J. Phys. Chem. C 118 (2014) 25097–25103, https://doi.org/10.1021/jp508454h.

[12] N.J. Waleska, F. Düll, P. Bachmann, F. Hemauer, J. Steinhauer, C. Papp, Reactivity and passivation of Fe nanoclusters on h-BN/Rh(111), Chem. - A Eur. J. (2021) 17087–17093, https://doi.org/10.1002/chem.202102590.

[13] T. Hill, M. Mozaffari-Afshar, J. Schmidt, T. Risse, S. Stempel, M. Heemeier, H.-J. Freund, Influence of CO adsorption on the magnetism of small Co particles deposited on Al2O3, Chem. Phys. Lett. 292 (1998) 524–530, https://doi.org/10.1016/S0009-2614(98)00690-3.

[14] R. Denecke, M. Kinne, C.M. Whelan, H.-P. Steinrück, In-situ core-level photoelectron spectroscopy of adsorbates on surfaces involving a molecular beam — General setup and first experiments, Surf. Rev. Lett. 09 (2002) 797–801, https://doi.org/10.1142/S0218625X0200297X.

[15] U. Muller, Inorganic Structural Chemistry, 2nd ed., John Wiley & Sons, 2006.

[16] F. Düll, M. Meusel, F. Späth, S. Schötz, U. Bauer, P. Bachmann, J. Steinhauer, H.-P. Steinrück, A. Bayer, C. Papp, Growth and stability of Pt nanoclusters from 1 to 50 atoms on h-BN/Rh(111), Phys. Chem. Chem. Phys. 21 (2019) 21287–21295, https://doi.org/10.1039/c9cp04095a.

[17] M. Corso, W. Auwärter, M. Muntwiler, A. Tamai, T. Greber, J. Osterwalder, Boron nitride nanomesh, Science 303 (2004) 217–220, https://doi.org/10.1126/science.1091979.

[18] J. Schmidt, T. Risse, H. Hamann, H.-J. Freund, Characterization of a model Ziegler–Natta catalyst for ethylene polymerization, J. Chem. Phys. 116 (2002) 10861–10868, https://doi.org/10.1063/1.1479722.

[19] F. Düll, U. Bauer, F. Späth, P. Bachmann, J. Steinhauer, H.-P. Steinrück, C. Papp, Bimetallic Pd-Pt alloy nanocluster arrays on graphene/Rh(111): formation, stability, and dynamics, Phys. Chem. Chem. Phys. 20 (2018) 21294–21301, https://doi.org/10.1039/c8cp03749c.

[20] C.J. Weststrate, J.W. Niemantsverdriet, CO adsorption on Co(0001) revisited: high-coverage CO superstructures on the close-packed surface of cobalt, J. Catal. 408 (2022) 142–154, https://doi.org/10.1016/j.jcat.2022.03.005.

[21] B. Tränkenschuh, C. Papp, T. Fuhrmann, R. Denecke, H.-P. Steinrück, The dissimilar twins - A comparative, site-selective in situ study of CO adsorption and desorption on Pt(322) and Pt(355), Surf. Sci. 601 (2007) 1108–1117, https://doi.org/10.1016/j.susc.2006.12.004.

[22] C.J. Weststrate, M. Mahmoodinia, M.H. Farstad, I.H. Svenum, M.D. Strømsheim, J. W. Niemantsverdriet, H.J. Venvik, Interaction of hydrogen with flat (0001) and corrugated (11–20) and (10–12) cobalt surfaces: insights from experiment and theory, Catal. Today 342 (2020) 124–130, https://doi.org/10.1016/j.cattod.2019.04.002.

[23] R. Gubo, P. Ren, X. Yu, T. Zhang, X. Wen, Y. Yang, Y.W. Li, J.W. Niemantsverdriet, C.J. Weststrate, Similarities and trends in adsorbate induced reconstruction – Structure and stability of FCC iron and cobalt surface carbides, Appl. Surf. Sci. 626 (2023) 157245, https://doi.org/10.1016/j.apsusc.2023.157245.

[24] C.J. Weststrate, D. Sharma, M.A. Gleeson, J.W. Niemantsverdriet, Water and hydroxyl reactivity on flat and stepped cobalt surfaces, J. Phys. Chem. C 127 (2023) 2974–2980, https://doi.org/10.1021/acs.jpcc.2c08425.

[25] T. Risse, A. Carlsson, M. Bäumer, T. Klüner, H.J. Freund, Using IR intensities as a probe for studying the surface chemical bond, Surf. Sci. 546 (2003) L829–L835, https://doi.org/10.1016/j.susc.2003.09.044.

[26] G.A. Beitel, A. Laskov, H. Oosterbeek, E.W. Kuipers, Polarization modulation infrared reflection absorption spectroscopy of CO adsorption on Co(0001) under a high-pressure regime, J. Phys. Chem. 100 (1996) 12494–12502, https://doi.org/10.1021/jp960045f.

[27] D.P. Woodruff, A.M. Bradshaw, Adsorbate structure determination on surfaces using photoelectron diffraction, Reports Prog. Phys. 57 (1994) 1029–1080, https://doi.org/10.1088/0034-4885/57/10/003.

[28] U. Bauer, C. Gleichweit, O. Höfert, F. Späth, K. Gotterbarm, H.-P. Steinrück, C. Papp, Reactivity studies of ethylene, benzene and cyclohexane on carbide-modified Mo(110) using high resolution X-ray photoelectron spectroscopy, Surf. Sci. 678 (2018) 11–19, https://doi.org/10.1016/j.susc.2018.01.001.

[29] K. Gotterbarm, C. Steiner, C. Bronnbauer, U. Bauer, H.-P. Steinrück, S. Maier, C. Papp, Graphene-templated growth of Pd nanoclusters, J. Phys. Chem. C 118 (2014) 15934–15939, https://doi.org/10.1021/jp5052563.
[30] M.D. Strømsheim, I.H. Svenum, M.H. Farstad, C.J. Weststrate, A. Borg, H.J. Venvik, CO-Induced surface reconstruction of the Co(11-20) surface - A combined theoretical and experimental investigation, J. Phys. Chem. C 124 (2020) 28488–28499, https://doi.org/10.1021/acs.jpcc.0c07852.
[31] R.L. Toomes, D.A. King, The adsorption of CO on Co{1010}, Surf. Sci. 349 (1996) 1–18, https://doi.org/10.1016/0039-6028(95)01049-1.